

EuCd₂As₂: a magnetic semiconductor

D. Santos-Cottin,^{1,*} I. Mohelský,² J. Wyzula,^{1,2} F. Le Mardelé,^{1,2} I. Kapon,³ S. Nasrallah,^{1,4} N. Barišić,^{4,5} I. Živković,⁶ J. R. Soh,⁶ F. Guo,^{7,6} K. Rigaux,^{7,6} M. Puppin,^{7,6} J. H. Dil,^{7,6} B. Gudac,⁵ Z. Rukelj,⁵ M. Novak,⁵ A. B. Kuzmenko,³ C. C. Homes,⁸ Tomasz Dietl,^{9,10} M. Orlita,^{2,11} and Ana Akrap^{1,†}

¹Department of Physics, University of Fribourg, CH-1700 Fribourg, Switzerland

²LNCMI, CNRS-UGA-UPS-INSA, 25, avenue des Martyrs, F-38042 Grenoble, France

³Department of Physics, University of Geneva, CH-1204 Geneva, Switzerland

⁴Institute of Solid State Physics, TU Wien, A-1040 Vienna, Austria

⁵Department of Physics, Faculty of Science, University of Zagreb, Bijenička 32, HR-10000 Zagreb, Croatia

⁶Institut de Physique, École Polytechnique Fédérale de Lausanne (EPFL), CH-1015 Lausanne, Switzerland

⁷Lausanne Centre for Ultrafast Science (LACUS),

École Polytechnique Fédérale de Lausanne (EPFL), CH-1015 Lausanne, Switzerland

⁸National Synchrotron Light Source II, Brookhaven National Laboratory, Upton, New York 11973, USA

⁹International Research Centre MagTop, Institute of Physics,

Polish Academy of Sciences, Aleja Lotnikow 32/46, PL-02668 Warsaw, Poland

¹⁰WPI Advanced Institute for Materials Research, Tohoku University,

2-1-1 Katahira, Aoba-ku, Sendai 980-8577, Japan

¹¹Institute of Physics, Charles University, CZ-12116 Prague, Czech Republic

(Dated: October 12, 2023)

EuCd₂As₂ is now widely accepted as a topological semimetal in which a Weyl phase is induced by an external magnetic field. We challenge this view through firm experimental evidence using a combination of electronic transport, optical spectroscopy and excited-state photoemission spectroscopy. We show that the EuCd₂As₂ is in fact a semiconductor with a gap of 0.77 eV. We show that the externally applied magnetic field has a profound impact on the electronic band structure of this system. This is manifested by a huge decrease of the observed band gap, as large as 125 meV at 2 T, and consequently, by a giant redshift of the interband absorption edge. However, the semiconductor nature of the material remains preserved. EuCd₂As₂ is therefore a magnetic semiconductor rather than a Dirac or Weyl semimetal, as suggested by *ab initio* computations carried out within the local spin-density approximation.

Magnetic Weyl semimetals have harboured the great hope of bringing spintronics and topology together, unfortunately, to a great extent only in theory. Candidate materials where the magnetic Weyl phase might come to fruition are scarce, and their solid experimental confirmations are even scarcer [1–5]. EuCd₂As₂ has been seen as one of a few rare magnetic Weyl semimetals – stable under ambient conditions, with large Eu spins positioned on a frustrated triangular lattice. The interplay of frustrated magnetism with topological bands made EuCd₂As₂ into a hopeful playground for a broad range of exciting phenomena [6, 7]. Through an extreme sensitivity of valence and conduction bands to Eu magnetism, external fields would then modify the band structure [8]. This compound has up to this point been proposed and interpreted as a Weyl semimetal, based upon *ab initio* band structure calculations, electronic transport and photoemission measurements [6, 8–10].

In this work, we study ultraclean EuCd₂As₂ crystals. Electronic transport measurements indicate an extremely low hole concentration. Accordingly, optical conductivity shows no detectable Drude component, and a strong Reststrahlen phonon mode. Our pump-probe photoemission measurement points to a clear band gap, and a carrier lifetime in the picosecond time scale. These experiments, together with extensive optical measurements,

provide decisive proof that EuCd₂As₂ is a semiconductor, and not a topological semimetal as previously thought [6, 9–13]. We deduce a band gap of 770 meV. Our results underline the need for more adapted band structure calculations. Moreover, our results demonstrate that the band structure of EuCd₂As₂ changes dramatically in an external magnetic field, due to an intimate coupling to localized Eu spins. All of these effects persist up to high temperatures, deep within the paramagnetic phase. We understand this through a strong exchange coupling of Eu 4*f* localized spins to the band states originating from Eu 6*s*, 6*p* and 5*d* orbitals.

Single crystals of EuCd₂As₂ were prepared by the Sn-flux method [6]. Details of sample synthesis, X-ray and electron probe microanalysis are described in Supplemental Material (SM) [14]. Carrier density was changed through controlling the purity of the starting materials. To increase the crystal size and quality, a two-step process was employed, where the crystals from the first growth were used as a seed material for the final growth. The layered trigonal lattice of EuCd₂As₂, shown in the inset of Fig. 1(a), results in triangular and hexagonally shaped crystals. The flux-growth of single crystals leads to an optically isotropic (001) surface. Blocks of Cd₂As₂ are sandwiched between the Eu planes, with similar distances to binary semiconducting CdAs₂ [15]. We have

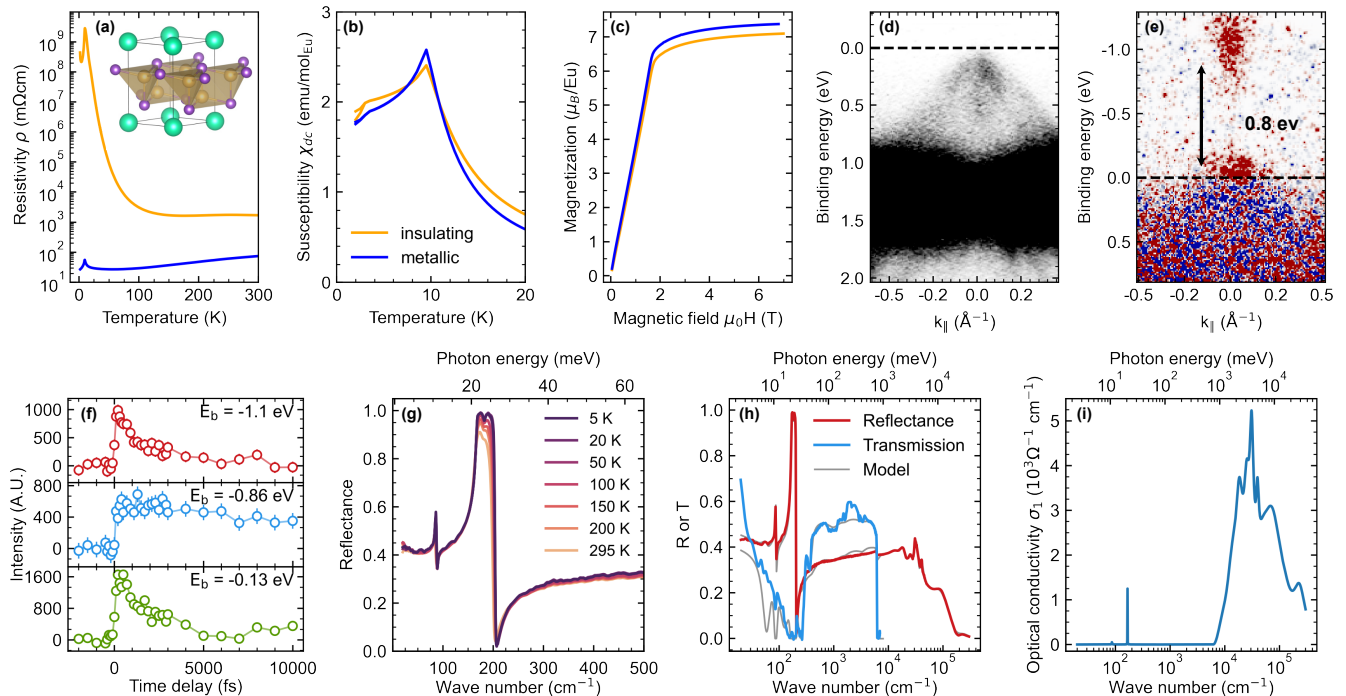


Figure 1. (a) Resistivity as a function of temperature for an insulating and a metallic sample. Inset shows the structure of EuCd_2As_2 , with Eu atoms shown in green, Cd atoms in yellow, and As atoms in purple. Magnetic properties, (b) dc susceptibility, and (c) magnetization at 4 K, are shown for the same two sample batches. (d) Static ARPES band map. (e) Pump-probe ARPES experiment results at a delay of 200 fs, where red means increased count rate after the pump-pulse excitation. (f) Time traces of the intensity integrated at different energies E_b above the Fermi level. The integration is done for a 200 meV window around the indicated energy. (g) Infrared reflectance at different temperatures, for the insulating sample batch. (h) Transmission and reflectance at 5 K, and their multilayer modelling, which results in (i) the real part of the optical conductivity, σ_1 .

determined infrared reflectance and transmission [16, 17], complemented by infrared measurements in magnetic fields up to 16 T, for details see SM [14]. Time-resolved photoemission (tr-ARPES) experiments were carried out at the EPFL LACUS, at the ASTRA end station [18] of the Harmonium beamline [19], with details described in SM [14].

Through a controlled crystal synthesis, we obtained insulating samples of EuCd_2As_2 , which have not been reported before. Figure 1(a) shows the resistivity of an insulating sample, resulting from a higher-purity synthesis, compared to a metallic sample, made through a standard purity synthesis. The resistivity of a high-purity sample is thermally activated above T_N , with an activation energy of ~ 30 meV, flattening above 170 K. Given the Hall coefficient sign, this indicates that thermal activation from the acceptor states is present up to 170 K and valence band transport above. A strong activation energy decrease in a magnetic field, and the corresponding colossal negative magnetoresistance, is expected for magnetic semiconductors in a paramagnetic phase [20, 21], in agreement with our resistivity in magnetic fields [14].

The standard synthesis results in metallic behavior above 50 K, consistent with previous reports. Interestingly, in both samples the resistivity peak at $T_N = 9.5$ K coincides with a sharp, symmetric peak in the magnetic susceptibility, χ_{dc} in Fig. 1(b), and an antiferromagnetic (AFM) ordering [9]. The susceptibility in both metallic and insulating samples shows no difference between the zero-cooled and field-cooled (measured in 10 mT) values above 3.5 K [14], excluding a possible ferromagnetic phase above T_N [22]. The magnetization $M(\mu_0H)$ is measured with the field applied along the c axis, perpendicular to the Eu planes. $M(\mu_0H)$ first steeply and linearly increases up to 0.8 T, followed by a kink at 1.8 T, reaching a saturated value of $\sim 7\mu_B/\text{Eu}$ atom. This corresponds to the divalent Eu with half filled $4f$ orbitals, like in EuTe [23]. The initial step slope of $M(\mu_0H)$ is consistent with a ferromagnetic structure within each layer, and a relatively weak magnetic anisotropy expected for atoms with a half-filled orbital. Despite a strong difference in the resistivity, the susceptibility and magnetization are very similar in both samples, implying a weak effect of residual doping on magnetic properties. Both samples

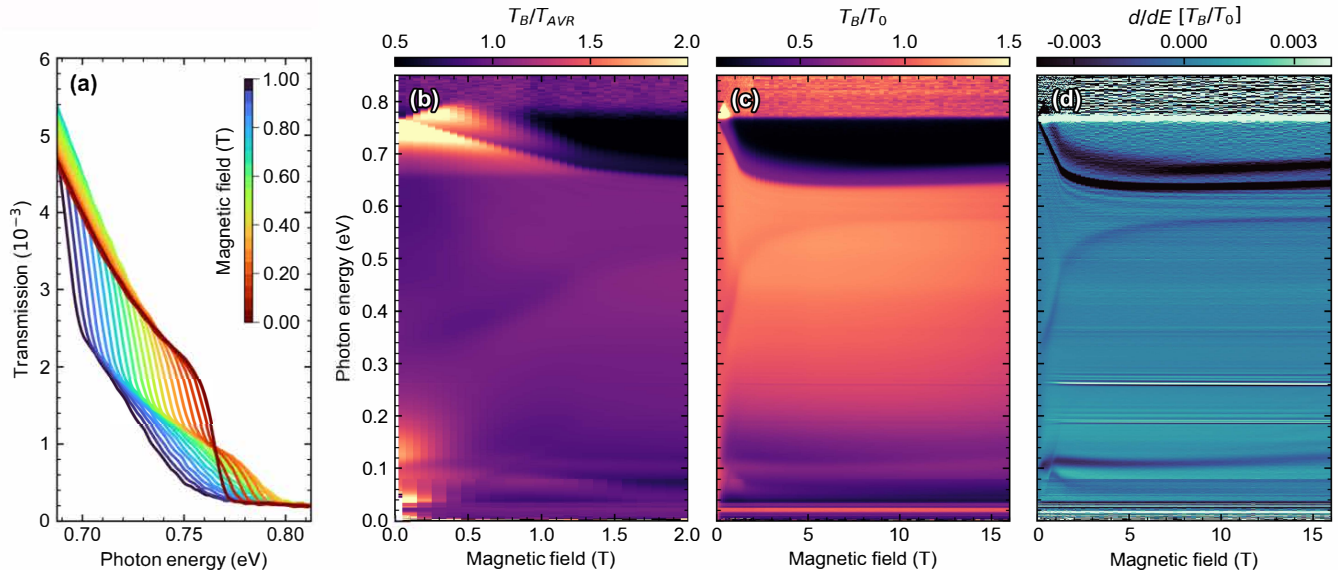


Figure 2. (a) Near infrared transmission showing the interband absorption edge at low fields, $B < 1$ T. (b) Color plot of relative magneto-transmission, T_B/T_{AVR} , in a broad energy range, and up to 2 T. (c) Magneto-transmission T_B/T_0 and (d) its first energy-derivative, $d/dE[T_B/T_0]$, in a broad energy and magnetic field range.

are insulating or at the localization boundary, meaning there are insufficient band carriers at low temperatures to change T_N by the RKKY mechanism.

The resistivity of the sample with lower residual doping strongly disagrees with the widely accepted notion that EuCd_2As_2 is a semimetal, and instead suggests it is a semiconductor. To confirm this, we turn to photoemission measurements of the more resistive samples. Figure 1(d) shows a static ARPES band map, where the band structure agrees with the published spectra [6, 8, 9]. A strong $4f^7$ band is centered around 1.3 eV below the Fermi level, and the valence band is near the Fermi level. The results of a pump-probe experiment in Fig. 1(e) show the conduction band minimum around 800 meV above the Fermi level. No further states are seen in the band gap under these conditions. The conduction band shows extremely high intensity and is visible without any data treatment. Time traces of the intensity integrated at different energies above the Fermi level are shown in Fig. 1(f). The valence band maximum at ~ 130 meV, and the conduction band away from the minimum, both show a time delay of around 1 ps. In contrast, the conduction band minimum ($E_b = -0.86$ eV) shows hardly any decay within the full observed time range of 10 ps. The long recombination time implies an energy barrier, and confirms there is a band gap of 770 ± 70 meV. Similar results are obtained on a metallic sample [14].

The infrared properties of EuCd_2As_2 are shown in Fig. 1(g-i), determined for the insulating sample. Far-infrared reflectance, shown at several different temperatures in Fig. 1(g), is dominated by two strong in-plane,

E_u phonon modes, at 86 and 165 cm^{-1} [24]. The higher frequency mode is an unscreened Reststrahlen mode, since there are no free carriers to screen it. The weak temperature dependence of the reflectance is typical of semiconductors. Moreover, the value of reflectance at low photon energies is far below unity, contrasting the behaviour of metals and semimetals. To obtain the precise value of the semiconducting band gap, we determine transmission through a thin EuCd_2As_2 sample. Transmission and reflectance are modelled using a multilayer model of the dielectric response [25]. Kramers-Kronig analysis of reflectance is unreliable as the sample is highly transparent in the mid-infrared range. The obtained optical conductivity, $\sigma_1(\omega)$, is shown in Fig. 1(i). The onset of absorption coincides with a sudden drop in transmission at 770 meV (6200 cm^{-1}). No Drude component appears in the optical conductivity, in line with our resistivity measurement. Metallic samples [14] show screened phonons, in agreement with previous optical studies [24, 26]. In metallic and insulating samples, the infrared phonons appear at the same frequencies, and there is a strong increase of the optical conductivity above 1 eV. In both cases, the Drude contribution, if at all present, is minor. Based on the experimental evidence outlined thus far, we assert that EuCd_2As_2 is a semiconductor—in our case with a light p -type doping—whose carrier density depends on the starting material purity and the crystal synthesis. The steep slope of the interband absorption edge at 770 meV is typical of a direct band gap [27]. This is consistent with the ARPES data in Fig. 1(e), showing the accumulation of both pho-

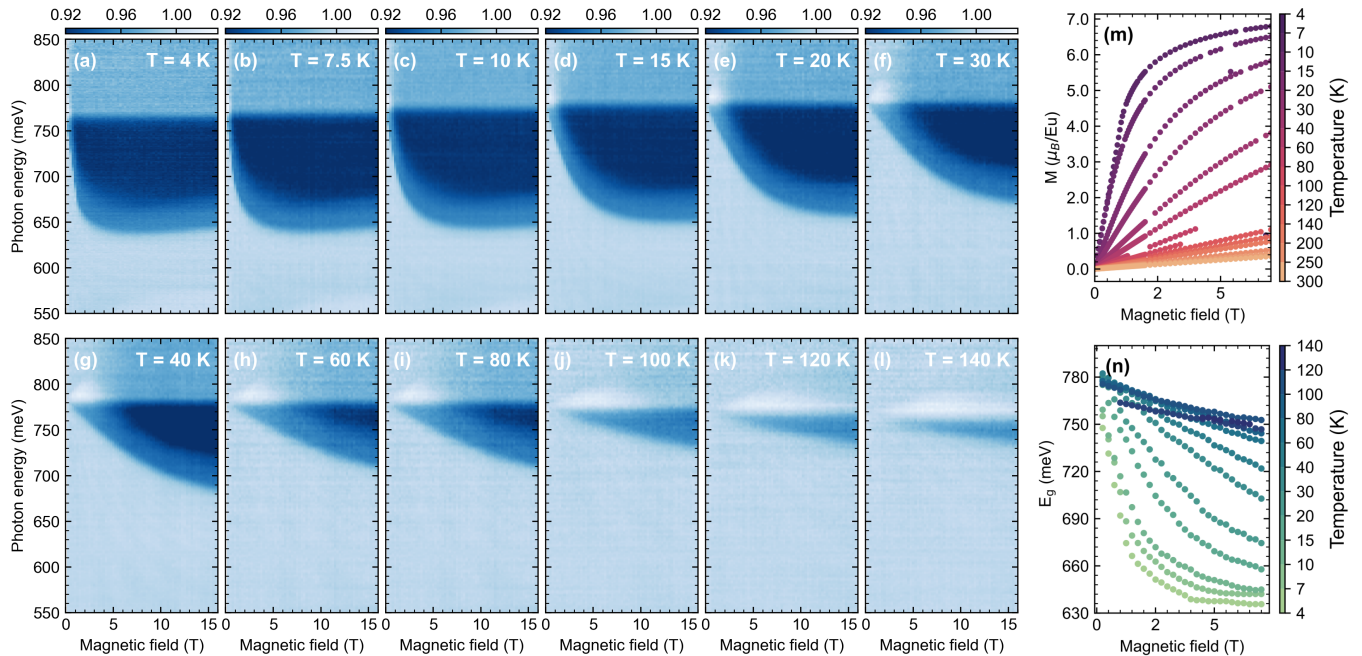


Figure 3. (a–l) Colorplots of relative infrared magneto-reflectivity, R_B/R_0 . Each panel represents a different temperature, going from the AFM phase below 9.5 K, deep into the paramagnetic phase. (m) Magnetization as a function of magnetic field, at the same set of temperatures where magneto-reflectivity is shown. (n) Onset of absorption extracted from the magneto-reflectivity color plots, at the same set of temperatures as in (m).

toexcited electrons and holes at the Γ point.

The electronic band structure of EuCd_2As_2 is remarkably tunable even with a small magnetic field. First, let us focus on the interband absorption edge, evident from magneto-transmission. In Fig. 2a, transmission spectra taken at 4 K are shown at photon energies around the onset, as the magnetic field is increased in 50 mT steps up to 1 T. Relative magneto-transmission in a broader energy and magnetic field range is shown in color plots in Fig. 2(b-d), where in (d) we show the energy-derivative of the magneto-transmission. Stacked plots of relative transmission are shown in the Supplemental Material [14]. The sharp zero-field step at 770 meV transforms into a double-step feature already at the lowest fields. Below 0.5 T, the lower energy step shifts down in energy, and the higher energy step moves up in energy. The steps split by 160 meV/T, giving an effective g factor with an extremely high value of ~ 1500 [28]. This large splitting originates from exchange interaction rather than Zeeman splitting. Above 0.5 T, the higher energy step also begins to redshift. The splitting between the two steps saturates at about 50 meV. This is a signature of spin polarized bands, which differently absorb light with opposite circular polarization. The weak oscillations of the signal below the gap, Fig 2(d), are assigned to giant Faraday rotation induced in our gapped system, with spin-split electronic bands, due to interband absorption of light that differs for opposite circular polarizations [14, 29, 30]. Remark-

ably, the band gap decreases by $\Delta E_g = 125$ meV under 2 T of applied field, reaching a plateau above 5 T.

While the gap is strongly reduced, it never closes in field, and no band inversion is seen. Instead, the strong redshift of the band gap $\Delta E_g(B)$ in Fig 2(b-d), is proportional to Eu spin magnetization $M(\mu_0 H)$, similarly to EuTe [31]. This means that the molecular field approximation is valid, and ΔE_g can be written as:

$$\Delta E_g = -\frac{1}{2} \mathcal{J}_{\text{eff}} S M(T, H) / M_S, \quad (1)$$

where \mathcal{J}_{eff} is an effective exchange energy between band carriers and Eu spins, $S = 7/2$, and M_S is saturated Eu spin magnetization. Highly localized $4f$ electrons will weakly hybridize with band states, and \mathcal{J}_{eff} originates mainly from the intraatomic potential exchange interaction. This interaction is ferromagnetic. According to optical spectra of free Eu^{1+} ions in the orbital momentum $L = 0$ state (no spin-orbit coupling), $\mathcal{J}_{6s-4f} = 52$, $\mathcal{J}_{6p-4f} = 33$ and $\mathcal{J}_{5d-4f} = 215$ meV [32, 33], in accord with chemical trends of $spd-f$ exchange energies determined for rare earths in solids [34]. Applying the above expression to our data, we obtain $\mathcal{J}_{\text{eff}} \approx 80$ meV. Therefore, we propose that the bands undergo a large splitting via $spd-f$ exchange coupling to Eu spins. Overall, our results provide a clear indication that the Eu magnetic sublattice controls the electronic band structure of the compound via a strong Eu onsite exchange interaction.

The natural question that follows is whether the observed effects are limited to the low-temperature AFM phase. Figure 3 shows a series of magneto-reflectivity color plots taken up to 16 T, at temperatures ranging from 4 to 140 K. In the magneto-reflectivity, we see the same kind of features as in the magneto-transmission: the band edge redshifting as magnetic field is applied, and a splitting between the upper and lower band gap edge. The zero-field band gap increases first, then decreases with increasing temperature. The splitting can be described by an effective g factor, which drops from 1500 at 4 K to 80 at 140 K [14]. At all the temperatures up to 100 K, we see that the bands become polarized in high magnetic field, even deep within the paramagnetic phase. This shows that EuCd_2As_2 is a strong paramagnet, and that qualitatively there is no difference in its response whether the zero-field state is an AFM or a paramagnet. Interestingly, at all temperatures, the extracted band edge as a function of external magnetic field behaves qualitatively very similar to magnetization, see Fig. 3(m-n). This means that the Eq. (1) remains valid for all temperatures and all magnetic fields.

In conclusion, with the full weight of the experimental evidence presented in this Letter, we show decisively that EuCd_2As_2 is not a topological semimetal, but rather a semiconductor with a band gap of 770 meV. This finding was verified on a number of specimens originating in five different syntheses. The absorption onset dependence on the magnetic field mimics the shape of magnetization. The band gap strongly decreases in magnetic fields, but it never becomes inverted, and the semiconductor nature of the material remains preserved. These results show that more accurate *ab initio* studies are desired, scrutinizing in detail all the complexities of correlated electron physics in Eu-based compounds [35]. Nonetheless, the local Eu magnetic moments are responsible for band structure changes, through strong $4f$ exchange coupling to valence and conduction states.

We thank B. Fauqué, M. Müller, D. van der Marel, N. Schröter, A. Grushin, F. de san Juan, Iurii Timrov and Luca Binci for enriching conversations. We are grateful to N. Miller for the helpful comments. A.A. acknowledges funding from the Swiss National Science Foundation through project PP00P2_202661. This research was supported by the NCCR MARVEL, a National Centre of Competence in Research, funded by the Swiss National Science Foundation (grant number 205602). F.G. and J.H.D. acknowledge the funding through SNSF grant 200021_200362. M.N. and N.B. acknowledge the support of CeNIKS project co-financed by the Croatian Government and the EU through the European Regional Development Fund Competitiveness and Cohesion Operational Program (Grant No. KK.01.1.1.02.0013). This work has been supported by the ANR DIRAC3D. We acknowledge the support of LNCMI-CNRS, a member of the European Magnetic Field Laboratory (EMFL). This work was sup-

ported by the Foundation for Polish Science through the International Research Agendas program co-financed by the European Union within the Smart Growth Operational Programme. The work at the TU Wien was supported by the European Research Council (ERC Consolidator Grant No 725521).

* david.santos@unifr.ch

† ana.akrap@unifr.ch

- [1] D. F. Liu, A. J. Liang, E. K. Liu, Q. N. Xu, Y. W. Li, C. Chen, D. Pei, W. J. Shi, S. K. Mo, P. Dudin, T. Kim, C. Cacho, G. Li, Y. Sun, L. X. Yang, Z. K. Liu, S. S. P. Parkin, C. Felser, and Y. L. Chen, *Science* **365**, 1282 (2019).
- [2] N. Morali, R. Batabyal, P. K. Nag, E. Liu, Q. Xu, Y. Sun, B. Yan, C. Felser, N. Avraham, and H. Beidenkopf, *Science* **365**, 1286 (2019).
- [3] S. Nie, T. Hashimoto, and F. B. Prinz, *Physical Review Letters* **128**, 176401 (2022).
- [4] J.-F. Wang, Q.-X. Dong, Z.-P. Guo, M. Lv, Y.-F. Huang, J.-S. Xiang, Z.-A. Ren, Z.-J. Wang, P.-J. Sun, G. Li, and G.-F. Chen, *Physical Review B* **105**, 144435 (2022).
- [5] M. Kanagaraj, J. Ning, and L. He, *Reviews in Physics* **8**, 100072 (2022).
- [6] J. Z. Ma, S. M. Nie, C. J. Yi, J. Jandke, T. Shang, M. Y. Yao, M. Naamneh, L. Q. Yan, Y. Sun, A. Chikina, V. N. Strocov, M. Medarde, M. Song, Y. M. Xiong, G. Xu, W. Wulfhekel, J. Mesot, M. Reticcioli, C. Franchini, C. Mudry, M. Müller, Y. G. Shi, T. Qian, H. Ding, and M. Shi, *Science Advances* **5**, eaaw4718 (2019).
- [7] Y. Xu, L. Das, J. Z. Ma, C. J. Yi, S. M. Nie, Y. G. Shi, A. Tiwari, S. S. Tsirkin, T. Neupert, M. Medarde, M. Shi, J. Chang, and T. Shang, *Physical Review Letters* **126**, 076602 (2021).
- [8] J. R. Soh, F. de Juan, M. G. Vergniory, N. B. M. Schröter, M. C. Rahn, D. Y. Yan, J. Jiang, M. Bristow, P. Reiss, J. N. Blandy, Y. F. Guo, Y. G. Shi, T. K. Kim, A. McCollam, S. H. Simon, Y. Chen, A. I. Coldea, and A. T. Boothroyd, *Physical Review B* **100**, 201102(R) (2019).
- [9] N. H. Jo, B. Kuthanazhi, Y. Wu, E. Timmons, T.-H. Kim, L. Zhou, L.-L. Wang, B. G. Ueland, A. Palasyuk, D. H. Ryan, R. J. McQueeney, K. Lee, B. Schrunck, A. A. Burkov, R. Prozorov, S. L. Bud'ko, A. Kaminski, and P. C. Canfield, *Physical Review B* **101**, 140402(R) (2020).
- [10] K. M. Taddei, L. Yin, L. D. Sanjeewa, Y. Li, J. Xing, C. dela Cruz, D. Phelan, A. S. Sefat, and D. S. Parker, *Physical Review B* **105**, L140401 (2022).
- [11] J. Ma, H. Wang, S. Nie, C. Yi, Y. Xu, H. Li, J. Jandke, W. Wulfhekel, Y. Huang, D. West, P. Richard, A. Chikina, V. N. Strocov, J. Mesot, H. Weng, S. Zhang, Y. Shi, T. Qian, M. Shi, and H. Ding, *Advanced Materials* **32**, 1907565 (2020).
- [12] J. R. Soh, C. Donnerer, K. M. Hughes, E. Schierle, E. Weschke, D. Prabhakaran, and A. T. Boothroyd, *Physical Review B* **98**, 064419 (2018).
- [13] J. R. Soh, E. Schierle, D. Y. Yan, H. Su, D. Prabhakaran, E. Weschke, Y. F. Guo, Y. G. Shi, and A. T. Boothroyd, *Physical Review B* **102**, 014408 (2020).
- [14] See Supplemental Material at

- <http://link.aps.org/supplemental/xxxx> for more information and data on sample synthesis and characterization; zero-field reflectance of metallic and insulating samples; expected temperature dependence of the Drude component in a semimetal; pump-probe ARPES measurement of a metallic sample; Faraday rotation; energy gap and the effective Landé factor; stacked plots of transmission and reflectivity in a magnetic field; resistivity in magnetic fields. The Supplemental Material includes the additional Refs. [27, 29, 36–40].
- [15] I. Schellenberg, U. Pfannenschmidt, M. Eul, C. Schwicker, and R. Pöttgen, *Zeitschrift für anorganische und allgemeine Chemie* **637**, 1863 (2011).
- [16] C. C. Homes, M. Reedyk, D. A. Cradles, and T. Timusk, *Applied Optics* **32**, 2976 (1993).
- [17] D. B. Tanner, *Physical Review B* **91**, 035123 (2015).
- [18] A. Crepaldi, M. Chergui, H. Berger, A. Magrez, P. Bugnon, F. van Mourik, J. Ojeda, C. A. Arrell, G. Gatti, S. Roth, and M. Grioni, *CHIMIA* **71**, 273 (2017).
- [19] J. Ojeda, C. A. Arrell, J. Grilj, F. Frassetto, L. Mewes, H. Zhang, F. van Mourik, L. Poletto, and M. Chergui, *Structural Dynamics* **3**, 023602 (2015).
- [20] J. Jaroszyński and T. Dietl, *Solid State Communications* **55**, 491 (1985).
- [21] T. Dietl, *Journal of the Physical Society of Japan* **77**, 031005 (2008).
- [22] A. Artmann, A. Mewis, M. Roepke, and G. Michels, *Zeitschrift für anorganische und allgemeine Chemie* **622**, 679 (1996).
- [23] N. F. Oliveira, S. Foner, Y. Shapira, and T. B. Reed, *Phys. Rev. B* **5**, 2634 (1972).
- [24] C. C. Homes, Z. C. Wang, K. Fruhling, and F. Tafti, *Physical Review B* **107**, 045106 (2023).
- [25] A. B. Kuzmenko, *Review of Scientific Instruments* **76**, 083108 (2005).
- [26] H. P. Wang, D. S. Wu, Y. G. Shi, and N. L. Wang, *Physical Review B* **94**, 045112 (2016).
- [27] P. Y. Yu and M. Cardona, *Fundamentals of Semiconductors* (Springer, Berlin Heidelberg, 2010).
- [28] R. Kirchschrager, W. Heiss, R. T. Lechner, G. Bauer, and G. Springholz, *Applied Physics Letters* **85**, 67 (2004).
- [29] L. Ohnoutek, M. Hakl, M. Veis, B. A. Piot, C. Faugeras, G. Martinez, M. V. Yakushev, R. W. Martin, Č. Drašar, A. Materna, G. Strzelecka, A. Hruban, M. Potemski, and M. Orlita, *Scientific Reports* **6**, 19087 (2016).
- [30] D. U. Bartholomew, J. K. Furdyna, and A. K. Ramdas, *Physical Review B* **34**, 6943 (1986).
- [31] L. E. Schmutz, G. Dresselhaus, and M. S. Dresselhaus, *Solid State Communications* **28**, 597 (1978).
- [32] H. N. Russell, W. Albertson, and D. N. Davis, *Physical Review* **60**, 641 (1941).
- [33] T. Dietl, C. Śliwa, G. Bauer, and H. Pascher, *Physical Review B* **49**, 2230 (1994).
- [34] H.-S. Li, Y. P. Li, and J. M. D. Coey, *Journal of Physics: Condensed Matter* **3**, 7277 (1991).
- [35] G. Cuono, R. M. Sattigeri, C. Autieri, and T. Dietl, “Ab-initio overestimation of the topological region in Eu-based compounds,” arXiv:2305.10804 (2023).
- [36] N. Doebelin and R. Kleeberg, *Journal of Applied Crystallography* **48**, 1573 (2015).
- [37] P. E. C. Ashby and J. P. Carbotte, *Phys. Rev. B* **89**, 245121 (2014).
- [38] B. Kuthanazhi, K. R. Joshi, S. Ghimire, E. Timmons, L.-L. Wang, E. Gati, L. Xiang, R. Prozorov, S. L. Bud’ko, and P. C. Canfield, *Physical Review Materials* **7**, 034402 (2023).
- [39] S. Von Molnar and S. Methfessel, *Journal of Applied Physics* **38**, 959 (1967).
- [40] Y. Tokura, *Reports on Progress in Physics* **69**, 797 (2006).

Supplemental Material for “EuCd₂As₂: a magnetic semiconductor ”

D. Santos-Cottin,¹ I. Mohelský,² J. Wyzula,^{1,2} F. le Mardelé,^{1,2} I. Kapon,³ S. Nasrallah,¹ N. Barišić,^{4,5}
 I. Živković,⁶ J.R. Soh,⁶ F. Guo,⁶ K. Rigaux,⁶ M. Puppin,⁶ J.H. Dil,⁶ B. Gudac,⁵ Z. Rukelj,⁵ M.
 Novak,⁵ A.B. Kuzmenko,³ C. C. Homes,⁷ Tomasz Dietl,^{8,9} M. Orlita,^{2,10} and Ana Akrap^{1,*}

¹Department of Physics, University of Fribourg, CH-1700 Fribourg, Switzerland

²LNCMI, CNRS-UGA-UPS-INSA, 25, avenue des Martyrs, F-38042 Grenoble, France

³Department of Physics, University of Geneva, CH-1204 Geneva, Switzerland

⁴Institute of Solid State Physics, TU Wien, A-1040 Vienna, Austria

⁵Department of Physics, Faculty of Science, University of Zagreb, Bijenička 32, HR-10000 Zagreb, Croatia

⁶Institut de Physique, École Polytechnique Fédérale de Lausanne, CH-1015 Lausanne, Switzerland

⁷Condensed Matter Physics and Materials Science Division,

Brookhaven National Laboratory, Upton, New York 11973, USA

⁸International Research Centre MagTop, Institute of Physics,

Polish Academy of Sciences, Aleja Lotnikow 32/46, PL-02668 Warsaw, Poland

⁹WPI Advanced Institute for Materials Research, Tohoku University, 2-1-1 Katahira, Aoba-ku, Sendai 980-8577, Japan

¹⁰Institute of Physics, Charles University in Prague, CZ-12116 Prague, Czech Republic

(Dated: October 11, 2023)

In the Supplemental Materials, we describe the sample synthesis in more detail, and show X-ray diffraction (XRD) and Electron Probe Microanalysis (EPMA) characterization. We provide information on zero-field optical properties for metallic samples in comparison to the insulating sample, presented in the main text. We show that the behavior expected for a semimetal, in particular the Drude component, is not observed in our samples. For a metallic sample, we show the time-resolved ARPES data, similar to the data for the insulating sample which are presented in the main text. We show Faraday rotation in a high magnetic field. Next, we show the temperature dependence of the band gap, and the effective g factor, extracted from the magneto-optical data in the main text. We also show that the band gap remains the same for samples made in different synthesis batches. Finally, we show the temperature dependence of the resistivity in magnetic fields.

SAMPLE SYNTHESIS AND CHARACTERIZATION

Our single crystals of EuCd₂As₂ were prepared by the Sn-flux method [1]. Starting materials were mixed in the ratio Eu:Cd:As:Sns = 1:2:2:10. Carrier density was changed through controlling the purity of the starting materials. Metallic samples were obtained by using lower purity (2N) Eu pieces packed under mineral oil. Insulating samples were obtained in a two-step process where the crystals from the initial growth were used as feeding material for the second (final) growth, while paying attention to Eu purity. The used Eu pieces were 4N purity, packed under Ar, and had a shiny metallic luster prior to being used. A similar synthesis was recently performed by another group [2]. Single crystals of EuCd₂As₂ were characterized by powder

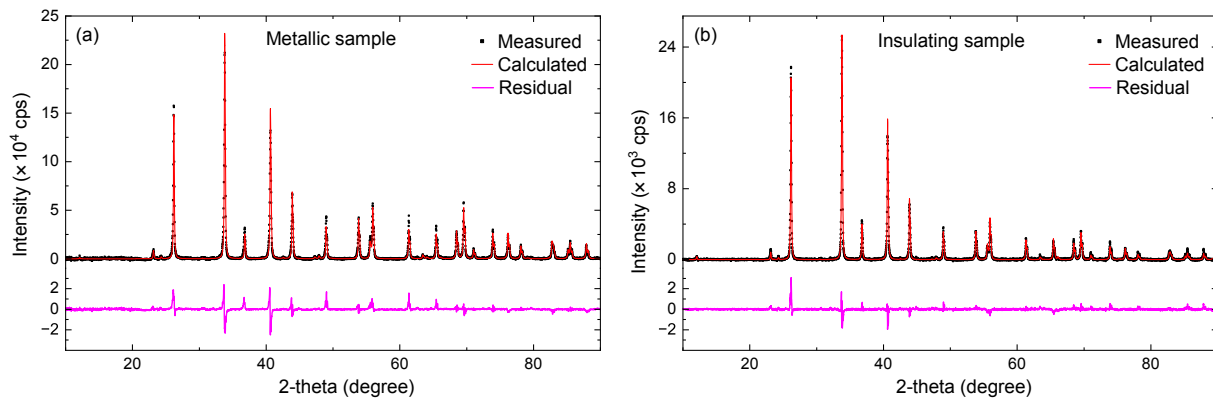


FIG. S1. Powder X-ray diffraction pattern of EuCd₂As₂ from the (a) metallic and (b) insulating batch. In both cases, the diffraction pattern confirms the structure of the trigonal crystal system with space group P-3m1 (no. 164). No traces of secondary phase or Sn flux have been detected.

X-ray diffraction and Electron Probe Microanalysis (EPMA).

For the powder X-ray diffraction, a few well-shaped crystals with no visible traces of Sn flux on the surface were selected from the metallic and insulating batch. The diffraction pattern in both cases was recorded in the range of 10-120 degrees, and the collected data were analyzed by the Rietveld refinement using Profex 5.2.0 software interface [3]. The analysis confirmed that the samples' structure belongs to the trigonal crystal system, with space group P-3m1 (no. 164), see Fig. S1. No visible traces of secondary phases were detected. The parameters of the refinement are given in Tables I and II.

For the insulating sample, we obtained the following lattice parameters: $a = 4.43956(6) \text{ \AA}$ and $c = 7.3266(1) \text{ \AA}$. For the metallic sample, we obtained: $a = 4.43995(6) \text{ \AA}$ and $c = 7.3274(2) \text{ \AA}$.

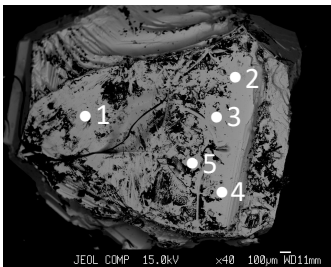
Most importantly, there is no change in the X-ray peak arrangement between the samples from the metallic and insulating batch.

| Atom | x | y | z |
|------|-----|-----|------------|
| Eu | 0 | 0 | 0 |
| Cd1 | 1/3 | 2/3 | 0.6327(2) |
| Cd2 | 1/3 | 2/3 | -0.6327(2) |
| As1 | 1/3 | 2/3 | 0.2483(3) |
| As2 | 1/3 | 2/3 | -0.2483(3) |

TABLE I. Atomic positions for the metallic sample obtained from XRD powder refinement.

| Atom | x | y | z |
|------|-----|-----|------------|
| Eu | 0 | 0 | 0 |
| Cd1 | 1/3 | 2/3 | 0.6317(2) |
| Cd2 | 1/3 | 2/3 | -0.6317(2) |
| As1 | 1/3 | 2/3 | 0.2556(3) |
| As2 | 1/3 | 2/3 | -0.2556(3) |

TABLE II. Atomic positions for the insulating sample obtained from XRD powder refinement.



| No. | Eu | Cd | As | Sn | Total |
|-----|---------|---------|---------|--------|-------|
| 1 | 20.5938 | 41.1180 | 41.0924 | 0.0691 | 100 |
| 2 | 20.2361 | 41.1950 | 38.5029 | 0.0660 | 100 |
| 3 | 20.7229 | 40.9689 | 38.2372 | 0.0710 | 100 |
| 4 | 20.3954 | 41.2546 | 38.2346 | 0.1154 | 100 |
| 5 | 20.5728 | 41.0924 | 38.2217 | 0.1131 | 100 |

FIG. S2. Electron Probe Microanalysis (EPMA) of a metallic EuCd_2As_2 single crystal. The analysis is done at several points on the crystal surface designated by numbers 1 to 5.

The EPMA was done on the as-synthesized metallic sample, as shown in Fig. S2. The composition was checked on multiple points on the sample surface, and it gave a good agreement with the stoichiometric ratio of $\text{Eu}:\text{Cd}:\text{As} = 1:2:2$. A small amount of Sn flux was detected on the sample's surface. This small amount of Sn flux results in a feature at 3.5 K in the magnetic susceptibility $\chi(T)$, which is due to the superconducting transition of Sn.

INFRARED SPECTROSCOPY, MAGNETO-TRANSMISSION AND MAGNETO-REFLECTIVITY EXPERIMENTS

Infrared reflectance and transmission were measured using a Bruker Vertex 80v spectrometer, at temperatures from 5 K to room temperature, with *in situ* gold evaporation [4]. High energy reflectance was complemented by ellipsometry and X-ray data [5]. The magneto-transmission and magneto-reflectivity were measured in the Faraday configuration, in magnetic fields up to

16 T, and at temperatures from 4 K to 140 K. The light wave vector propagated parallel to the external magnetic field, aligned with the crystallographic c axis. A Bruker Vertex 80v interferometer using an infrared source was coupled to the experiment using light-pipe optics. The sample was located in a superconducting coil and surrounded by the helium exchange gas.

TIME-RESOLVED PHOTOEMISSION EXPERIMENTS

Time-resolved photoemission (tr-ARPES) experiments were carried out at the EPFL LACUS, at the ASTRA end station [6] of the Harmonium beamline [7]. A single s -polarized harmonic at an energy of 37 eV was selected by a time-preserving monochromator. The *in situ* cleaved sample was excited by an s -polarized pump pulse at a fluence of 0.5 mJ/cm². The measurements were carried out at 80 K, with a temporal resolution better than 150 fs, an energy resolution of 150 meV, and an angular resolution of 0.3°.

ZERO-FIELD REFLECTANCE OF METALLIC AND INSULATING SAMPLES

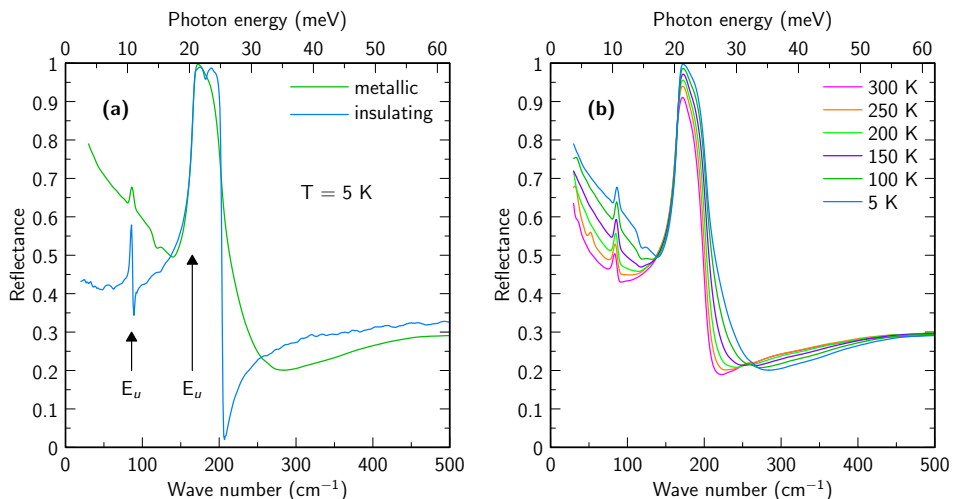


FIG. S3. (a) Reflectance of an insulating and a metallic sample at 5 K, and (b) reflectance of a metallic sample at various temperatures. The arrows in (a) point to the two infrared-active E_u phonon modes. Those modes are observed at the same frequencies, 86 and 165 cm⁻¹, in both of our samples, and agree well with the previous work on a metallic sample [8].

The optical reflectance at 5 K is shown for the metallic and insulating samples of EuCd₂As₂ in Fig. S3(a). In both cases, the dominant features are the two infrared active phonons of E_u symmetry, at 86 and 165 cm⁻¹, the latter forming a characteristic Reststrahlen band typical of semiconductors [9]. These frequencies agree well with the previous optical studies of EuCd₂As₂ [8]. The metallic sample shows a low-energy reflectance upturn, where $R \rightarrow 1$ as $\hbar\omega \rightarrow 0$, and is similar to the previous results [8]. This low-energy upturn is indicative of a weak Drude contribution in the metallic samples. Figure S3(b) shows the reflectance of the metallic sample at various temperatures, again consistent with the previous results [8]. We note that the low-energy reflectance *decreases* with temperature T . This is at odds with the expected semimetallic behavior, as we discuss below.

PUMP-PROBE ARPES MEASUREMENT OF A METALLIC SAMPLE

For a metallic sample, in Fig. S6 we show the static and pump-probe ARPES data. The data was taken in the same way as the data for the insulating sample, described and shown in the main text.

The chemical potential is now deeper inside the valence band, in agreement with the metallic resistivity shown in the main text, in Fig. 1(a). The bottom of the conduction band can be clearly resolved in the pump-probe spectra. Most important information is that, within the error bar, the band gap is the same as in the insulating sample, 0.7 ± 0.1 eV.

The gap is determined from the distance between the valence band maximum and the conduction band minimum and the error bars are based on the experimental energy resolution.

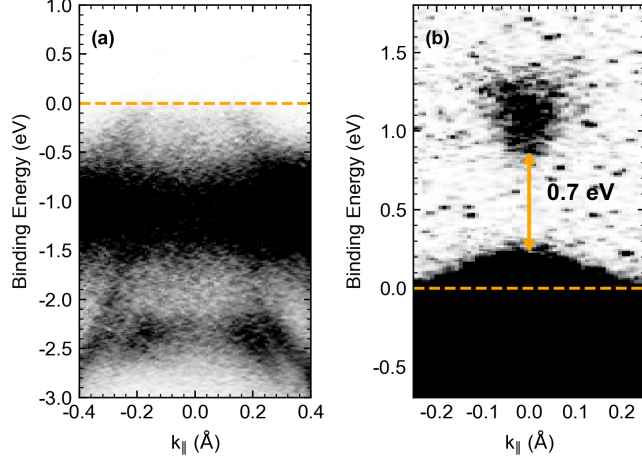


FIG. S4. (a) Static ARPES map of a metallic sample of EuCd_2As_2 . (b) Pump-probe ARPES spectrum on the same metallic sample, showing the conduction band, separated from the valence band by a sizeable gap.

TEMPERATURE DEPENDENCE OF THE DRUDE COMPONENT IN A SEMIMETAL

In a semimetal, the Drude component is expected to increase with T , contrary to what is seen in the previously published work on EuCd_2As_2 [8], as well as in our data.

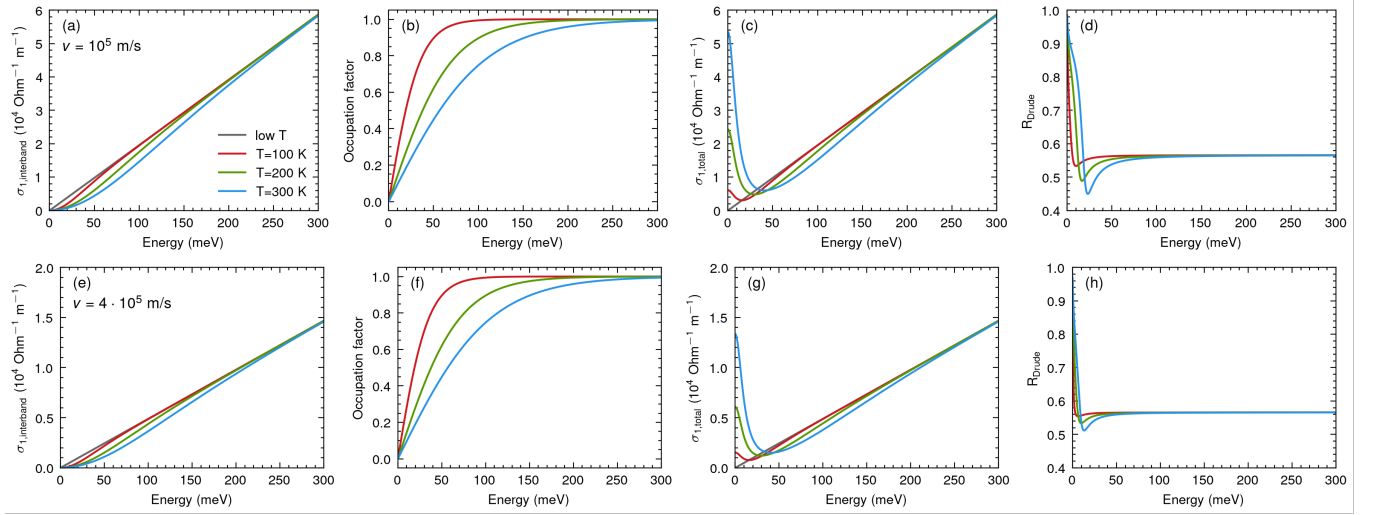


FIG. S5. Panels (a) and (e) show the interband optical conductivity calculated for two different Fermi velocities, 10^5 and 4×10^5 m/s. In (b) and (f) we show the occupational factor. Panels (c) and (g) show the total optical conductivity, which is a sum of the Drude term and the interband contribution. In (d) and (h) we show the calculated reflectance for the Drude part alone, showing the plasma edge which shifts to higher energies as the temperature increases.

To illustrate the expected semimetallic behavior, we provide readers with a quantitative estimate of the Drude contribution to optical conductivity, and its temperature dependence, in an ideal Weyl semimetal with two cones. For simplicity, we consider a full electron-hole symmetry and the Fermi level that crosses the Weyl nodes. The latter condition implies that the Drude weight vanishes at low temperatures. The optical conductivity at $T = 0$ can then be calculated using the expression by Ashby and Carbotte [10], which only reflects interband excitations:

$$\text{Re } \sigma_W(\omega) = n_{\text{valley}} \frac{e^2}{24\pi\hbar v} \omega. \quad (1)$$

Here, $n_{\text{valley}} = 2$ is the valley degeneracy, v is the velocity parameter, and ω is the photon frequency. At higher temperatures, the above expression has to be complemented by the occupation factor, $[f_D(-\hbar\omega/2) - f_D(\hbar\omega/2)]$, where f_D stands for the Fermi-Dirac distribution.

The result is shown in Figs. S5(a) and (e) at $T = 0, 100, 200$ and 300 K and for two different velocity parameters, 1×10^5 and 4×10^5 m/s. These two values represent velocity parameters typical of Weyl semimetals. With increasing T , the occupation factor – plotted separately in Figs. S5(b) and (f), for clarity – gradually suppresses the strength of interband excitations at low photon energies. This is due to a simple occupation effect that reflects electrons excited thermally from the valence to the conduction band. The thermally excited charge carries, both electrons and holes, give rise to a Drude-type part of optical conductivity, whose strength equals the thermally suppressed contribution of interband excitations. The resulting real part of optical conductivity, comprising both the Drude and interband excitations, is plotted in Figs. S5(c) and (g). Here we assumed the characteristic broadening of 10 meV for the Drude peak.

To estimate the impact of the thermally-induced Drude component on the overall optical response at low photon energies, we have calculated the corresponding reflectivity spectra, again as a function of T and for two characteristic values of the velocity parameter, see Figs. S5(d) and (h). To simplify our calculations, we have only included the Drude contribution, complemented by a background dielectric constant ($\epsilon_1 = 100$). We see that the thermally excited carriers give rise to a pronounced plasma-edge feature in the calculated reflectivity spectra. Hence, even though it is absent at low temperatures, the Drude contribution becomes relevant at higher temperatures and it is expected to impact profoundly the optical response at $T = 300$ K.

Let us note that this behavior – quantitatively evaluated for the case of an ideal Weyl semimetal – should be characteristic of any gapless phase, or even of weakly gapped systems, provided that the gap is significantly smaller than $k_B T$. The thermally induced Drude contribution should always be present at higher T , with the weight that reflects the particular profile of the (joint) density of states at low energies. On the other hand, the thermally-activated Drude component should stay negligible in systems with the energy band gap that is significantly larger than $k_B T$. This latter scenario is consistent with our data and also with the previous work on EuCd_2As_2 [8]. We observe neither a temperature increase in the Drude component, nor a development and increase of a plasma edge.

FARADAY ROTATION

In the main text, the magneto-transmission shows weak oscillations below the band gap, see Fig. 2(d) of the main text. These

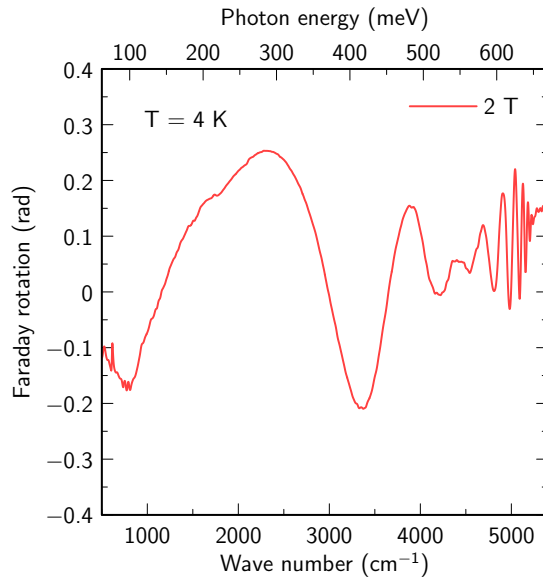


FIG. S6. Faraday rotation measured at 4 K and 2 T.

oscillations are related to the Faraday rotation. Faraday rotation measures how much polarization of the incident beam is rotated by the sample in a magnetic field.

EuCd_2As_2 is a gapped system, which becomes spin-polarized in a magnetic field. The two circular polarizations of light are absorbed differently. These two polarizations are mixed in our magneto-transmission measurements, but are separate in the measurement of Faraday rotation, shown in Fig. S6. We see that the Faraday rotation shows strong oscillations below the

band gap, similar to Bi_2Se_3 [11]. Hence, the left and right circularly polarized light is not equally absorbed, which manifests as oscillations in the magneto-transmission.

ENERGY BAND GAP AND THE EFFECTIVE g FACTOR

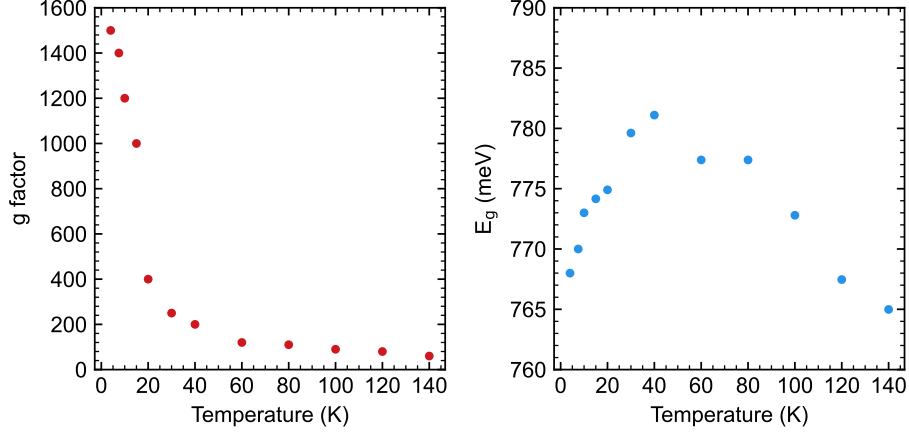


FIG. S7. (a) Effective g factor and (b) band gap, both as a function of temperature, extracted from the temperature-dependent relative magneto-reflectance.

The effective g factor and band gap can be extracted from the temperature dependent magneto-optical reflectivity, shown in the Fig. 3(a–l) of the main text. The resulting values are shown in Fig. S7. The large drop of the effective g factor takes place as the magnitude of magnetization at given magnetic field decreases rapidly with temperature above T_N . From 4 to 40 K, the band gap increases as the temperature increases. Above 40 K, the band gap decreases as the temperature grows.

STACKED PLOTS OF TRANSMISSION AND REFLECTIVITY IN A MAGNETIC FIELD

In the main text, we show color plots of relative magneto-transmission (Fig. 2b–d) and magneto-reflectance (Fig. 3a–l). Below, in Figures S8 and S9 we show the same data as a series of stacked plot made out of individual curves. For clarity, some of the data is omitted.

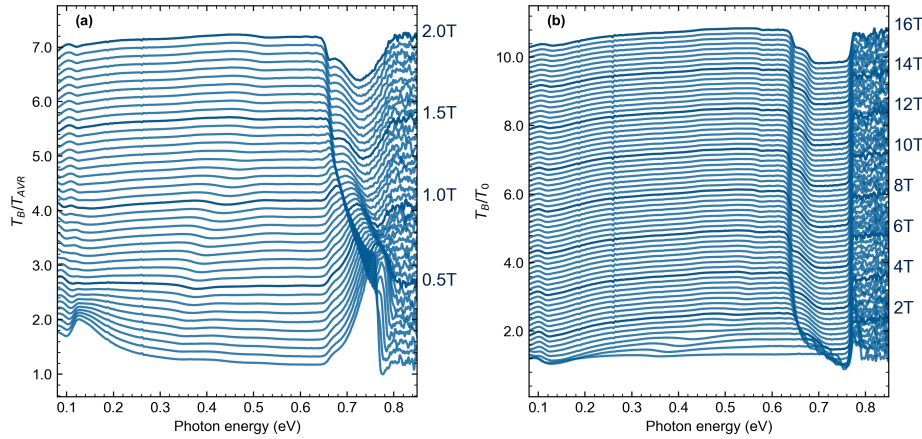


FIG. S8. Relative magneto-transmission shown up to the field of (a) 2 T and (b) 16 T, as a function of incident photon energy. Magneto-transmission is normalized by a field-average in (a) and by zero-field transmission T_0 .

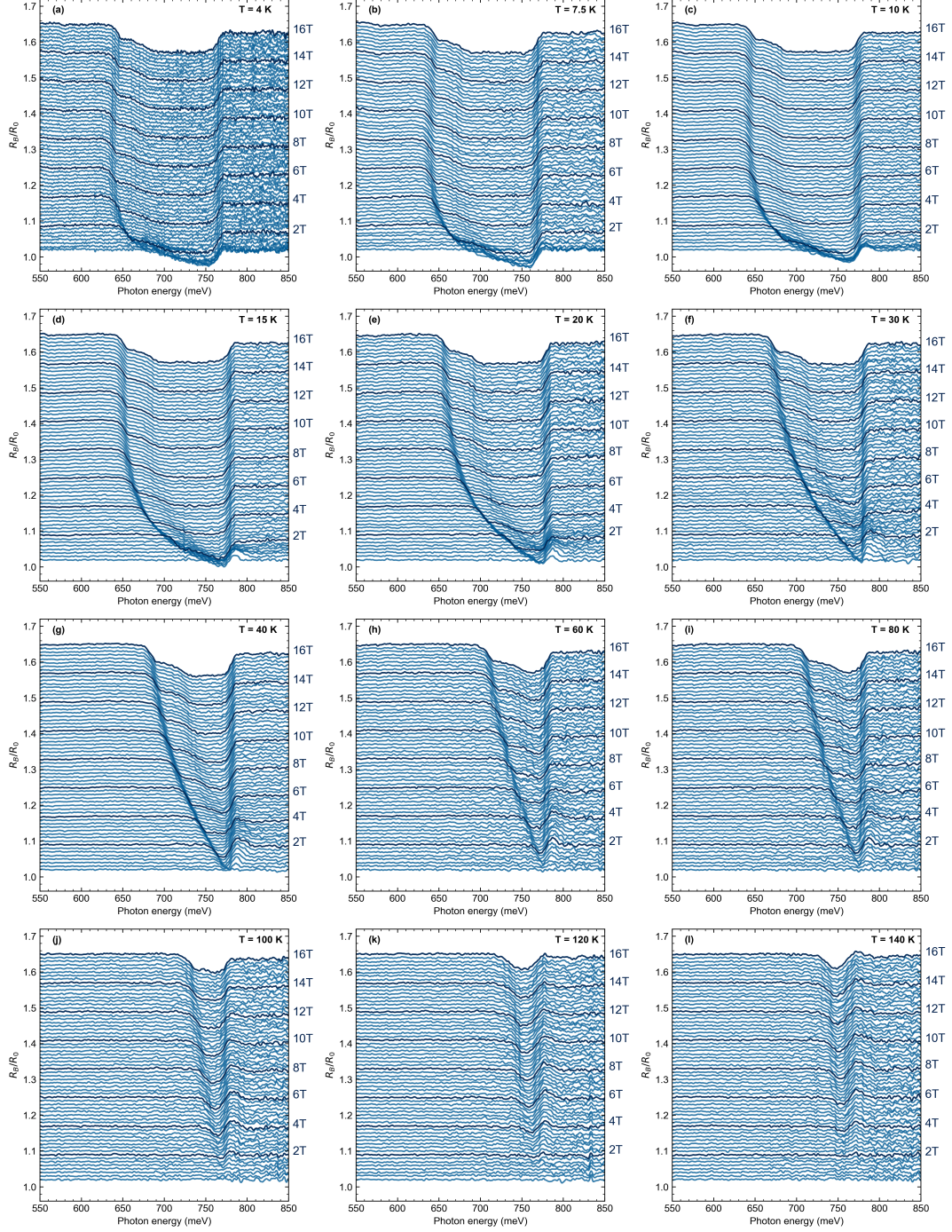


FIG. S9. Relative magneto-reflectivity, normalized by the zero-field reflectivity R_0 , and shown up to the field of 16 T for a series of different temperatures.

COMPARISON OF MAGNETO-OPTICAL DATA FOR DIFFERENT SAMPLES

The same band gap is present in all the samples we have measured. In Fig. S10 we show results of magneto-optical measurements performed on six samples coming from five different single crystal syntheses. Samples (c-f) are from the same synthesis batch. Sample (a-b) is discussed in the main text. In all the measurements, there is a clear and strong feature near 0.77 eV (or 6200 cm^{-1}) for the field $B = 0$ T. This feature corresponds to the band gap. The band gap changes very similarly in all the

measured samples, strongly decreasing in field.

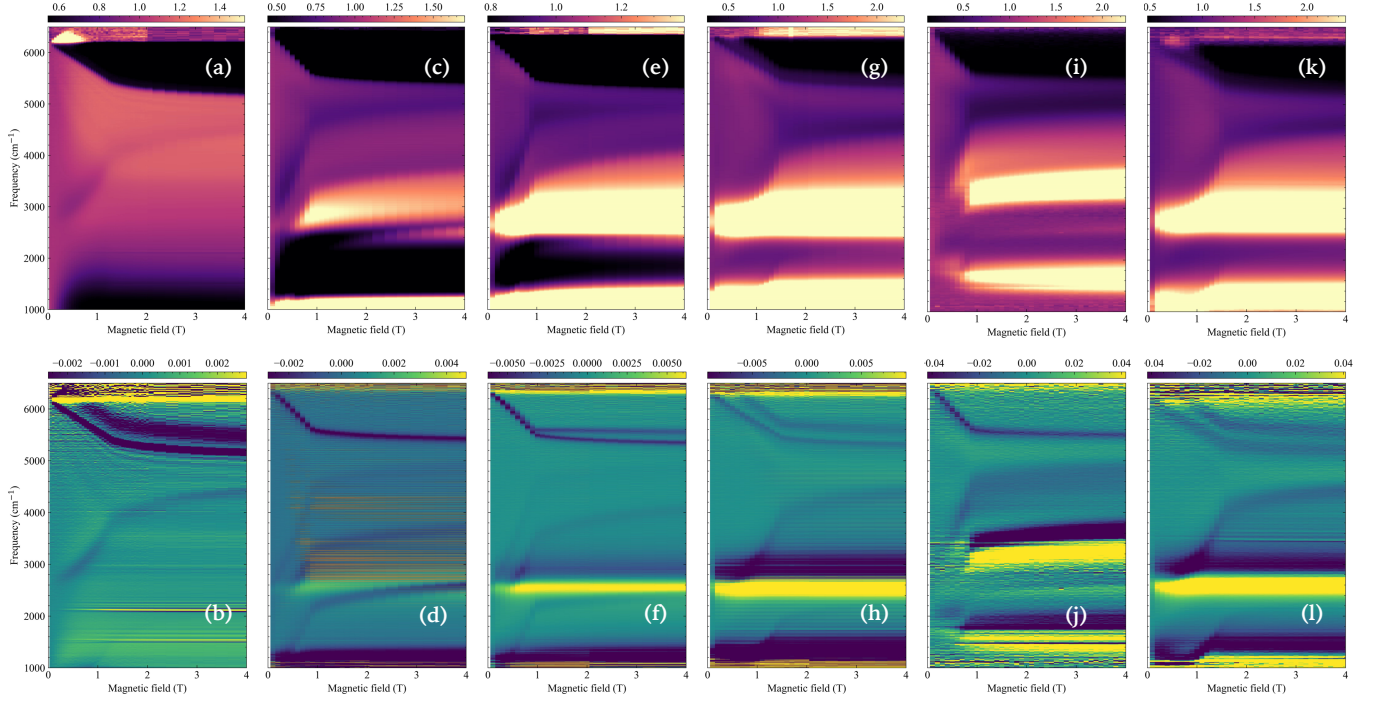


FIG. S10. (a,c,e,g,i,k) Magneto-transmission T_B/T_0 and (b,d,f,h,j,l) its first energy-derivative, $d/dE[T_B/T_0]$, shown in a broad energy up to magnetic field of 4 T.

RESISTIVITY IN MAGNETIC FIELDS

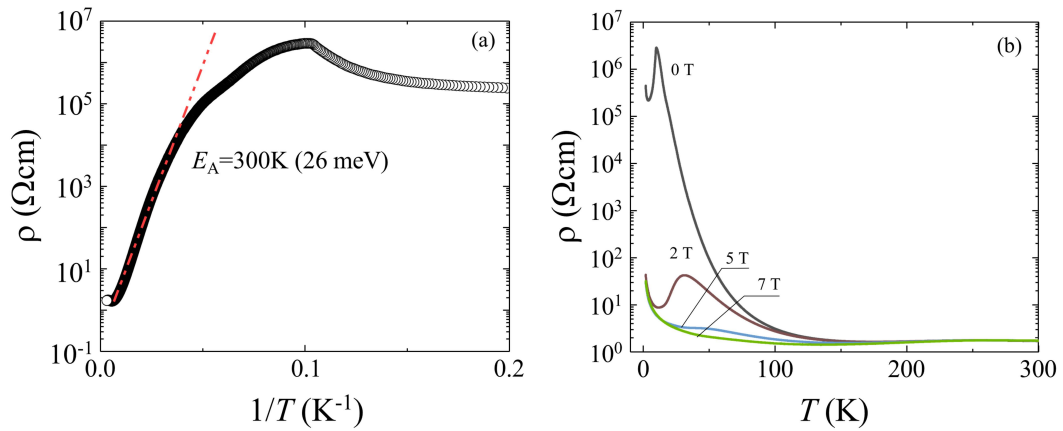


FIG. S11. (a) Resistivity showing activated behavior, with activation of 26 meV. (b) Resistivity in different magnetic fields, up to 7 T.

In the main text, we show the resistivity of an insulating and a metallic sample. Figure S11(a) shows the Arrhenius plot for the resistivity of an insulating sample, with the activation energy of 26 meV, in the temperature range 25 – 175 K. In a magnetic field, Fig. S11(b), the resistivity drops several orders of magnitude, but remains activated at low temperature, without

becoming metallic. Interestingly, a similar profound drop in the resistivity, spanning several orders of magnitude, was observed in a magnetic field in other insulating (gapped) magnetic systems, e.g., based on europium [12] or manganese [13].

* ana.akrap@unifr.ch

- [1] J. Z. Ma, S. M. Nie, C. J. Yi, J. Jandke, T. Shang, M. Y. Yao, M. Naamneh, L. Q. Yan, Y. Sun, A. Chikina, V. N. Strocov, M. Medarde, M. Song, Y. M. Xiong, G. Xu, W. Wulfhekkel, J. Mesot, M. Reticcioli, C. Franchini, C. Mudry, M. Müller, Y. G. Shi, T. Qian, H. Ding, and M. Shi, *Science Advances* **5**, eaaw4718 (2019).
- [2] B. Kuthanazhi, K. R. Joshi, S. Ghimire, E. Timmons, L.-L. Wang, E. Gati, L. Xiang, R. Prozorov, S. L. Bud'ko, and P. C. Canfield, *Physical Review Materials* **7**, 034402 (2023).
- [3] N. Doebelin and R. Kleeberg, *Journal of Applied Crystallography* **48**, 1573 (2015).
- [4] C. C. Homes, M. Reedyk, D. A. Cradles, and T. Timusk, *Applied Optics* **32**, 2976 (1993).
- [5] D. B. Tanner, *Physical Review B* **91**, 035123 (2015).
- [6] A. Crepaldi, M. Chergui, H. Berger, A. Magrez, P. Bugnon, F. van Mourik, J. Ojeda, C. A. Arrell, G. Gatti, S. Roth, and M. Gioni, *CHIMIA* **71**, 273 (2017).
- [7] J. Ojeda, C. A. Arrell, J. Grilj, F. Frassetto, L. Mewes, H. Zhang, F. van Mourik, L. Poletto, and M. Chergui, *Structural Dynamics* **3**, 023602 (2015).
- [8] H. P. Wang, D. S. Wu, Y. G. Shi, and N. L. Wang, *Physical Review B* **94**, 045112 (2016).
- [9] P. Y. Yu and M. Cardona, *Fundamentals of Semiconductors* (Springer, Berlin Heidelberg, 2010).
- [10] P. E. C. Ashby and J. P. Carbotte, *Phys. Rev. B* **89**, 245121 (2014).
- [11] L. Ohnoutek, M. Hakl, M. Veis, B. A. Piot, C. Faugeras, G. Martinez, M. V. Yakushev, R. W. Martin, Č. Drašar, A. Materna, G. Strzelecka, A. Hruban, M. Potemski, and M. Orlita, *Scientific Reports* **6**, 19087 (2016).
- [12] S. Von Molnar and S. Methfessel, *Journal of Applied Physics* **38**, 959 (1967).
- [13] Y. Tokura, *Reports on Progress in Physics* **69**, 797 (2006).